System analysis and controller design for the electric pump of a deep-throttling rocket engine

Hu, Runsheng; Ferrari, Riccardo M.G.; Chen, Zhenyu; Cheng, Yuqiang; Zhu, Xiaobin; Cui, Xing; Wu, Jianjun

DOI
10.1016/j.ast.2021.106729

Publication date
2021

Document Version
Final published version

Published in
Aerospace Science and Technology

Citation (APA)
Hu, R., Ferrari, R. M. G., Chen, Z., Cheng, Y., Zhu, X., Cui, X., & Wu, J. (2021). System analysis and controller design for the electric pump of a deep-throttling rocket engine. *Aerospace Science and Technology*, *114*, Article 106729. https://doi.org/10.1016/j.ast.2021.106729

Aerospace Science and Technology 114 (2021) 106729

Contents lists available at ScienceDirect

Aerospace Science and Technology

www.elsevier.com/locate/aescte

System analysis and controller design for the electric pump of a deep-throttling rocket engine

Runsheng Hu [a], Riccardo M.G. Ferrari [b], Zhenyu Chen [c], Yuqiang Cheng [a], Xiaobin Zhu [a], Xing Cui [a], Jianjun Wu [a,*]

[a] College of Aerospace Science and Engineering, National University of Defense Technology, Changsha, Hunan, 410073, People's Republic of China
[b] Delft Center for Systems and Control, Faculty of Mechanical, Maritime and Materials Engineering, Delft University of Technology, 2628 CD Delft, the Netherlands
[c] State Key Laboratory of Alternate Electrical Power, School of Control and Computer Engineering, North China Electric Power University, Beijing, 102206, People's Republic of China

ARTICLE INFO

Article history:
Received 11 November 2020
Received in revised form 25 March 2021
Accepted 6 April 2021
Available online 13 April 2021
Communicated by Choon Ki Ahn

Keywords:
Electric pump
Proportional-integral-derivative controller
Gain-scheduling linear quadratic regulator
Nonlinearity
Gap metric

ABSTRACT

This paper proposes a controller design for the electric pump of a deep-throttling rocket engine. The nonlinearity of the system is taken into consideration by analyzing the gap metric. Then, proportional-integral-derivative controller and gain-scheduling linear quadratic regulator are designed. Analyzing the amplitude- and phase-frequency characteristics as well as the pole-zero distribution of the system, the results show that the designed controllers can stabilize the linearized equations in incremental form at different operating points. This indicates that these two controllers are available for the original system in the whole range of working conditions and this is verified in the simulation. Meanwhile, the comparison between proportional-integral-derivative controller and gain-scheduling linear quadratic regulator is presented. It demonstrates that the proportional-integral-derivative controller is better at tracking both step and ramp signals but with worse control signals. It means that the proportional-integral-derivative controller seems less suitable for real use due to severe oscillations. Meanwhile, the parameter tuning of a proportional-integral-derivative controller depends on more extensive manual tuning. Therefore, the gain-scheduling linear quadratic regulator is preferred.

1. Introduction

Liquid-propellant rocket engines (LREs) are the main power equipment used for space transportation systems and spacecraft propulsion and maneuver [1,2]. Liquid-propellant rocket engine with thrust that can be varied in a wide range has gained much importance in recent years. Its diversified developments have put forward many novel requirements in the aerospace field [3]. Variable-thrust rocket engine makes a good candidate for space exploration and transport, such as manned lunar landing and Mars exploration [3,4], as it can change thrust on-demand. In order to meet the requirement of soft landing, variable thrust technology with a wide range in descent phase is necessary. Throttleable LREs undoubtedly play a significant role in this kind of mission, especially for lunar descent. On the one hand, there is no air or the air is extremely rarefied. On the other hand, the engine needs to balance the gravity of the vehicle with decreasing mass and the acceleration of gravity over a wide range of variations. Therefore, the LREs must have the ability of deep throttling.

The propellant types or compositions, the propellant mass flow rates, the nozzle exit area, and the nozzle throat area contribute to throttle a single engine. However, it is difficult to change the propellants, the nozzle exit area, and the nozzle throat area due to physical restrictions or heat flux. As we know, the thrust of the rocket engine is mainly calculated as the sum of the momentum thrust and the differential-pressure thrust in the steady state. The momentum thrust is the product of the propellant mass flow rate and the exhaust velocity. While the differential-pressure thrust is the product of the nozzle exit area and the pressure difference between the outlet pressure of the exhaust and the atmospheric pressure. Therefore, the rocket engine thrust varies with the propellant mass flow rate approximately in a linear relation. Consequently, regulating the propellant mass flow rates is the simplest way to regulate engine thrust [5].

There are mainly eight throttling approaches [5], which are high-pressure-drop injectors, dual-manifold injectors, gas injection, multiple chambers, pulse modulation, variable area injectors,

* Corresponding author.
E-mail address: jjwu@nudt.edu.cn (J. Wu).

https://doi.org/10.1016/j.ast.2021.106729
1270-9638/

Nomenclature

PID	proportional, integral and derivative
LQR	linear quadratic regulation
UAV	unmanned air vehicle
LREs	liquid-propellant rocket engines
EPPS	electric propellant pump system
LOX	liquid oxygen
DC	direct current
U_m	supply voltage of the motor
R_m	resistance of the circuit
i_m	current
L_m	inductance
t	time
e_m	back electromotive force
C_e	back electromotive coefficient of the motor
ω	rotational angular velocity of the motor
M	output torque of the motor
C_m	torque coefficient of the motor
J_m	equivalent rotational inertia of the motor
f_m	equivalent viscous friction coefficient of the motor
M_c	load torque of the motor
n	rotational speed
$\dot{m}$	mass flow rate
$\dot{m}_r$	reference mass flow rate
n_r	reference rotational speed
N_i, M_i	right normalized coprime fractions
$\tilde{N}_i, \tilde{M}_i$	left normalized coprime fractions
k_p	proportional coefficient
k_i	integral coefficient
k_d	derivative coefficient
N	filter coefficient
x	state variables of the system
u	input of the system
$\dot{x}$	derivatives of the state variables
y	output of the system
e	error between the real output and desired one
$\mathbf{K}$	gain matrix of the controller
$\mathbf{Q}$	weighting matrix for state increment
$\mathbf{R}$	weighting matrix for control signal increment
MSE	mean square error
ITAE	integrated time and absolute error
ITSE	integral time square error
GA	genetic algorithm
PSO	particle swarm optimization
AMS	aerial manipulation systems
RMSE	root mean square error

hydro-dynamically dissipative injectors, and also the combined methods mentioned above. All of these methods have both merits and shortage.

Stable and efficient combustion process in a rocket engine is the key factor for the safety and reliability of space programs [6]. In order to have a better atomization to get a satisfying combustion efficiency and adequate resistance for system performance, it is important to keep the injector with a constant injection pressure drop during the whole throttling process [7]. One effective method to solve the problem is to regulate the propellant mass flow rate and change the injection area simultaneously [8]. In view of this point, turbopump feed system is often applied to modulating propellant mass flow rate as it ensures a light weight design for a liquid rocket engine. However, it is also with the drawbacks of mechanical complexity and the ensuing limited reliability (e.g., a large fraction of launch failures is due to malfunctioning turbopump systems) [9]. Therefore, in this paper, the assembled motor and pump was adopted to regulate the propellant mass flow rate.

Small centrifugal pumps have been designed, manufactured and performance tested in the 1980s [10] in the frame of a development program for an Electric Propellant Pump System (EPPS) for storable propellants. Compared with a pressure-fed system, EPPS used on a communication satellite makes the weight and volume of the propellant system reduced. Beyond its application to aircraft and satellites, several studies in the early 2000s used electrically driven pump-fed cycle engines for launch vehicles [11]. Besides, the propellant electric pump designed for delivering liquid hydrogen or methane to the rocket engine was one of the core project topics [12]. In reference [11], performance assessment, including combustion chamber pressure, burning time, thrust level, mass as well as payload capability, of electrically driven pump-fed LOX/kerosene cycle rocket engine was presented. Compared with pressure-fed and turbopump-fed systems, the specific mass of the electric-pump system can be reduced. This makes the system competitive, at least for some applications such as small launchers and upper stage rockets [13]. Meanwhile, advanced batter cells currently under development could make the system lighter than the turbopump one, even for applications involving short burning times, i.e., booster stages [13].

The rest of the paper is organized as follows. In section 2, the model of the electric pump is mentioned. Section 3 analyzes the nonlinearity of the system and section 4 details the controller design process. Next section presents the simulation results. Finally, conclusions are drawn in section 6.

2. Dynamics modeling

The electric pump studied in this paper consists of two parts, i.e., direct current (DC) motor and the centrifugal pump.

DC motor transfers the electrical energy into mechanical energy. By inducing electromagnetic torque through the interaction between current and coil, it drives the load, i.e. pump, to rotate. The dynamics equations of DC motor mainly comprise three parts, i.e., the voltage balance equation, the electromagnetic torque equation, and the torque equilibrium equation.

The voltage balance equation of the motor in the armature circuit can be expressed as

$$U_m = L_m \frac{di_m}{dt} + i_m R_m + e_m \tag{1}$$

where U_m is the supply voltage of the motor, R_m is the resistance of the circuit, i_m is the current, L_m is the inductance, t is the time, and e_m is the back electromotive force, which can be calculated by

$$e_m = C_e \omega \tag{2}$$

where C_e is the back electromotive coefficient of the motor and ω is the rotational angular velocity of the motor.

The electromagnetic torque equation of the motor is

$$M = i_m C_M \tag{3}$$

where M is the output torque of the motor and C_M is the torque coefficient of the motor.

The torque equilibrium equation of the motor is

$$J_m \frac{d\omega}{dt} + f_m \omega = M - M_c \tag{4}$$

where J_m is the equivalent rotational inertia of the motor, f_m is equivalent viscous friction coefficient of the motor, and M_c is the load torque of the motor by which the pump is driven to work. In this case, the load torque M_c can be written as

$$M_c = kn^2 \tag{5}$$

where k is a constant and n is the rotational speed.

As we know, the rotational speed and rotational angular speed hold a relationship as follows

$$n = \frac{30\omega}{\pi} \tag{6}$$

Here we assume that the mass flow rate of the pump is proportional to the rotational speed, thus the mass flow rate provided by the pump can be calculated by

$$\dot{m} = \dot{m}_r \frac{n}{n_r} \tag{7}$$

where $\dot{m}_r$ and n_r are the reference mass flow rate and rotational speed, respectively. In this paper, $\dot{m}_r$ is 1.35 kg/s and n_r is 40000 rpm.

3. System nonlinearity analysis

The motor characterized by Eq. (1) and (4) is a typical second-order linear system and can be easily controlled by a proportional-integral (PI) or proportional-integral-derivative (PID) controller. The controller can be designed according to the state-space form equation to obtain a satisfactory control effect.

However, the quadratic load torque (Eq. (5)) is added to Eq. (4) in our study. Considering Eq. (1)-(6), we could obtain

$$\frac{di_m}{dt} = -i_m \frac{R_m}{L_m} - \omega \frac{C_e}{L_m} + \frac{U_m}{L_m} \tag{8}$$

$$\frac{d\omega}{dt} = i_m \frac{C_m}{J_m} - \omega \frac{f_m}{J_m} - \omega^2 \frac{k}{4\pi^2 J_m} \tag{9}$$

The quadratic term, ω^2, representing the load torque driving the pump to work, brings nonlinearity to the system.

Combined with Eq. (6) and (7), Eq. (8) and (9) can be written as

$$\frac{di_m}{dt} = -i_m \frac{R_m}{L_m} - \dot{m} \frac{\pi n_r C_e}{30 \dot{m}_r L_m} + \frac{U_m}{L_m} \tag{10}$$

$$\frac{d\dot{m}}{dt} = i_m \frac{30 \dot{m}_r C_m}{\pi n_r J_m} - \dot{m} \frac{f_m}{J_m} - \dot{m}^2 \frac{30 k n_r}{\pi \dot{m}_r J_m} \tag{11}$$

Selecting $\dot{m}$ as the output, the following output equation is obtained.

$$y = \dot{m} \tag{12}$$

As the electric pump is a nonlinear system, the nonlinearity of the system needs to be analyzed, such that a suitable control scheme can be designed. Here, the gap metric is adopted to weigh the nonlinearity of the system and it will be discussed in the following.

The gap metric was introduced into control field as it was an effective way to study the uncertainty in feedback systems [14, 15]. The gap metric can characterize the difference between two linear systems. If the gap metric is close to 0, this means these two systems have similar dynamic responses. While if the gap metric is close to 1, the two systems' dynamic responses are apart. For two linear systems, P_1 and P_2, the gap metric between them is defined as

$$\delta(P_1, P_2) = \max\left(\vec{\delta}(P_1, P_2), \vec{\delta}(P_2, P_1)\right) \tag{13}$$

where

$$\vec{\delta}(P_1, P_2) = \inf_{Q \in H_\infty} \left\| \begin{bmatrix} N_1 \\ M_1 \end{bmatrix} - \begin{bmatrix} N_2 \\ M_2 \end{bmatrix} Q \right\|_\infty \tag{14}$$

where Q belongs to RH_∞, and N_i and M_i are the right or left normalized coprime fractions as follows (if N_i and M_i have no common factors or common roots, they are coprime):

$$P_i = N_i M_i^{-1} = \tilde{M}_i^{-1} \tilde{N}_i \tag{15}$$

For a nonlinear system,

$$\dot{x} = f(x, u) \tag{16}$$

$$y = h(x, u), \tag{17}$$

the linearized system in incremental form at $x = x_0$, $u = u_0$ can be expressed as follows

$$\Delta\dot{x} = \frac{\partial f(x,u)}{\partial x}|_{f(x_0,u_0)} \Delta x + \frac{\partial f(x,u)}{\partial u}|_{f(x_0,u_0)} \Delta u \tag{18}$$

$$\Delta y = \frac{\partial h(x,u)}{\partial x}|_{h(x_0,u_0)} \Delta x + \frac{\partial h(x,u)}{\partial u}|_{h(x_0,u_0)} \Delta u \tag{19}$$

According to Eq. (10)-(12), the linearized system can be derived as

$$\begin{bmatrix} \Delta\dot{x}_1 \\ \Delta\dot{x}_2 \end{bmatrix} = \begin{bmatrix} -\frac{R_m}{L_m} & -\frac{\pi n_r C_e}{30 \dot{m}_r L_m} \\ \frac{30 \dot{m}_r C_m}{\pi n_r J_m} & -\frac{f_m}{J_m} - \frac{60 k n_r}{\pi \dot{m}_r J_m} x_2|_{x_2 = x_{2,0}} \end{bmatrix} \begin{bmatrix} \Delta x_1 \\ \Delta x_2 \end{bmatrix} + \begin{bmatrix} \frac{1}{L_m} \\ 0 \end{bmatrix} \Delta u \tag{20}$$

$$\Delta y = \begin{bmatrix} 0 & 1 \end{bmatrix} \begin{bmatrix} \Delta x_1 \\ \Delta x_2 \end{bmatrix} \tag{21}$$

In order to measure the nonlinearity of the electric pump system, several operating points were selected and the system was linearized at given operating points. Then the gap metrics between two linearized systems was obtained.

The variable range of mass flow rate is $\dot{m} \in [0, 1.35]$ kg/s. First, we gridded the operating space by using N = 136 operating points: the gap metrics thus calculated are illustrated in Fig. 1 (the Y-axis is the same as X-axis and they both denote the mass flow rate). The maximum gap metric is 0.3997. Then we gridded the operating space by N = 135 operating points and $\dot{m}$ changing from 0.01 kg/s to 1.35 kg/s. Gap metrics calculated for $\dot{m} \in [0.01, 1.35]$, instead, are illustrated in Fig. 2. Finally we gridded the operating space by N = 101 operating points and $\dot{m}$ varying from 0 kg/s to 0.01 kg/s: gap metrics calculated are illustrated in Fig. 3.

Fig. 1-3 demonstrated that when $\dot{m}$ changes from 0 kg/s to 0.01 kg/s, the gap metrics have a substantial increase. Except the conditions near the operating point where the mass flow rate equals to 0, the gap metrics are rather small. When the mass flow rate equals to 0, it is the start or the end of the operation and we have no demand to maintain this condition. Therefore, the operating points near $\dot{m} = 0$ play less important roles compared with other conditions which need to work for a long period. We can tolerant larger tracking errors at these instants as they last a negligible amount of time and their effect on the trajectory are null. In general, the gap metric between any two linearized systems in incremental form is small and the closed-loop behaviors can be quite close. This demonstrates the nonlinearity of the whole system is not strong and the nonlinearities between two different operating points are continuous. Therefore, it is a good choice to adopt either linear approximation or gain-scheduling controllers.

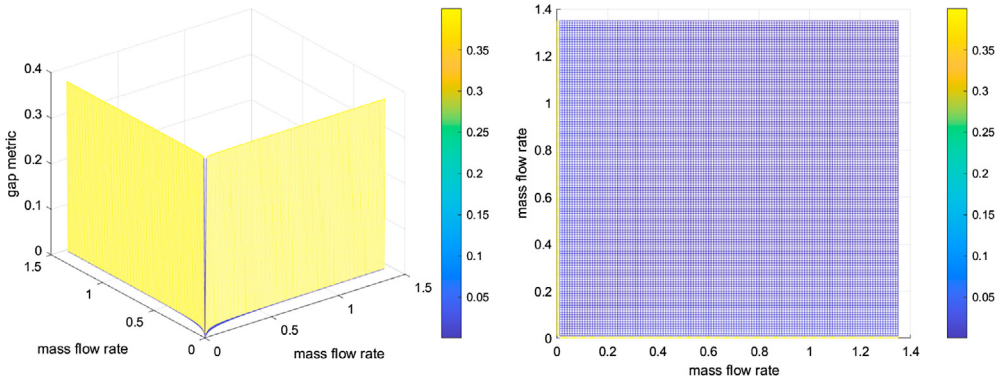

(a) Isometric view (b) Top view

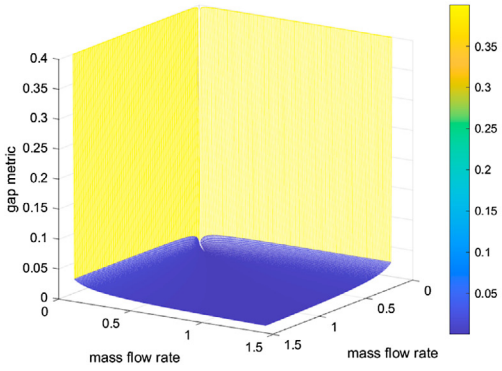

(c) Rear view of the isometric view

Fig. 1. Gap metric surface of the system ($\dot{m} \in [0, 1.35]$). (For interpretation of the colors in the figure(s), the reader is referred to the web version of this article.)

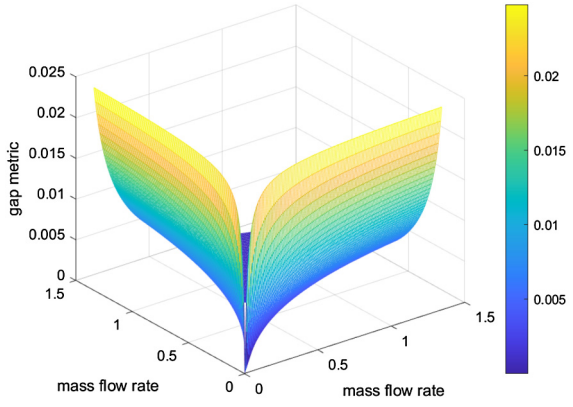

Fig. 2. Gap metric surface of the system ($\dot{m} \in [0.01, 1.35]$).

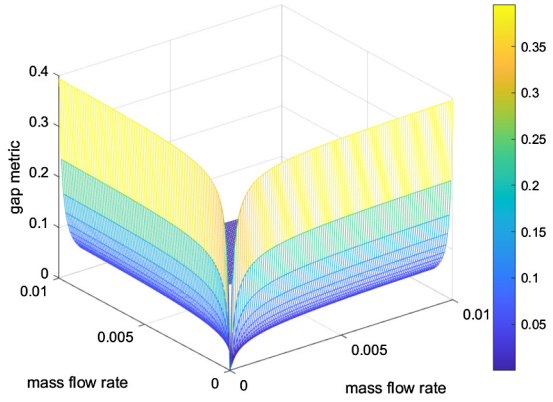

Fig. 3. Gap metric surface of the system ($\dot{m} \in [0, 0.01]$).

4. Controller design

4.1. Proportional-integral-derivative controller

The Proportional-integral-derivative (PID) controller is shown to be the simplest and most efficient way to cope with many industrial-implementation-oriented control problems. Because its proportional coefficient can decrease the rising time of response, integral coefficient can reduce the steady-state errors, and derivative coefficient can improve the transient response like overshoot [16]. In reference [17], a PID controller was utilized in order to make a stable flow of fluid in the pipelines by controlling the vibration in an electric pump. PID controller can cope with not only linear control problems, but also problems with moderate nonlinearities, especially for the PID controller with auto-tuning gains. A conventional PID was applied to generate control inputs for a nonlinear unsteady aerodynamics model [18]. This model is coupled with a three degree of freedom quadplane to control the forward and backward transition between hover and steady level flight. In reference [19], an anti-skid PID braking control system was used on a nonlinear dynamic landing gear model to capture gear walk. Based on a novel PID controller with a Nussbaum-type function, a

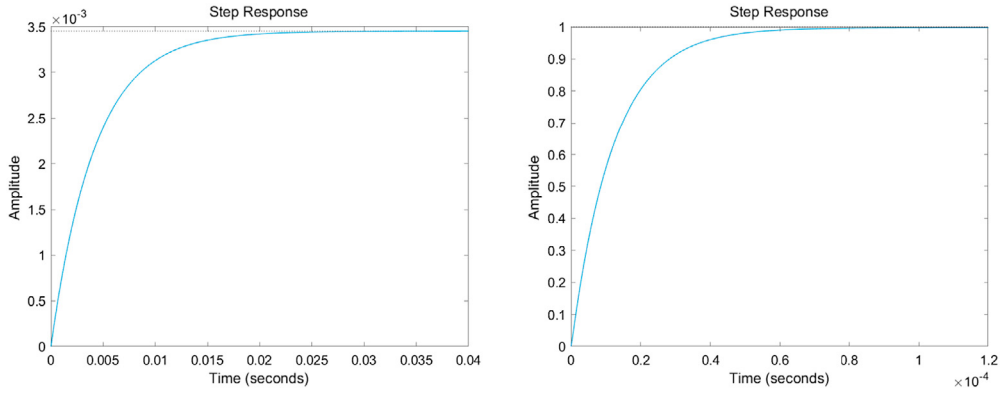

(a) Without the PID controller (b) With the PID controller

Fig. 4. Step responses of the linearized system at full working condition.

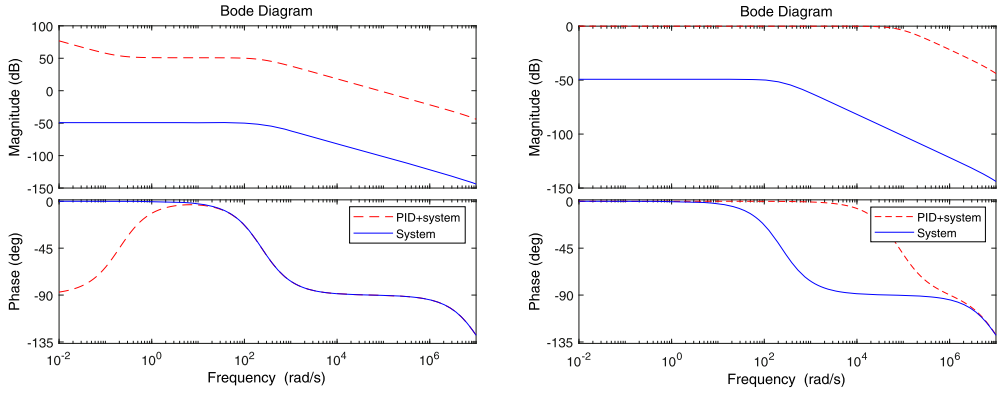

(a) Open loop Bode plot (b) Close loop Bode plot

Fig. 5. Bode plots of the linearized system at full working condition.

robust adaptive and fault-tolerant control scheme was developed for wind turbines [20]. By utilizing the Nussbaum-type function and the matrix decomposition technique to adaptively tune gains, the PID control could be made robust, adaptive, and fault-tolerant, and applicable to nonlinear systems with uncertainties and unexpected actuation faults [21]. As the nonlinearity of the electric pump system is not strong, a traditional PID controller can be used here.

According to the linearized system at full working condition ($\dot{m} = 1.35$ kg/s), a PID controller is designed as follows

$$u = k_p + k_i \frac{1}{s} + k_d \frac{N}{1 + N\frac{1}{s}} \tag{22}$$

where k_p is the proportional coefficient, k_i is the integral coefficient, k_d is the derivative coefficient, and N is the filter coefficient, which equal to 1e5, 2e4, 0.5, and 100, respectively. Parameters in the PID controller are tuned following industrial tuning rules, which are based on the adjust time and overshoot. For example, in order to reduce the rise time of system response, we can mainly increase the value of k_p. If we want to have a small steady-state error, we can increase the value of k_i. While when we want to reduce the overshoot of the response, we can increase the value of k_d. As a matter of fact, optimization-based PID tuning is also conducted during our controller design. Mean square error (MSE), integrated time and absolute error (ITAE) and integral time square error (ITSE) were used as the cost function by which the PID parameters were optimized using genetic algorithm (GA) or particle swarm optimization (PSO) algorithm. However, it was shown that the optimization results were unacceptable. Usually, optimization-based PID tuning can be adopted to determine the PID parameters. However, special characteristic of the studied object in this paper makes it difficult. Due to its nonlinearity, the optimum PID parameters at different operating conditions are not the same. Single objective optimization can result in a long rising time or a long time to reach steady state for one or more operating conditions. In fact, multi-objective optimization based PID tuning might be helpful. This may need further study. Due to the listed reasons, in this work, the industrial tuning procedure is used and a sub-optimal but satisfactory solution is achieved. After tuning, the close-loop system with the PID controller is shown to have a good tracking ability as required while maintaining the responses under constraints.

At the full working condition, the state-space matrices of the linearized system are listed below, and the step responses as well as Bode plots are shown in Fig. 4 and 5. The settling time of the step response with the PID controller, which is in the order of tens of microseconds, is far less than that without the controller, on the order of tens of milliseconds, as plotted in Fig. 4(a) and (b). From Fig. 4, we can also find that the steady-state value with the PID controller is 1 while the steady-state value without the

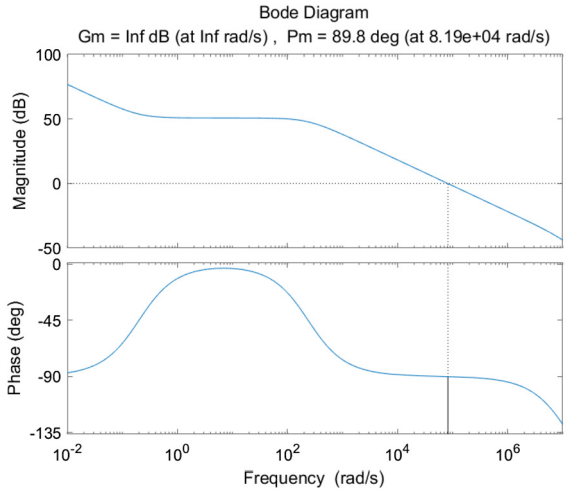

Fig. 6. Phase and magnitude margin of the linearized system with the PID controller at full working condition.

PID controller is 3.5e-3. The steady-state error with the PID controller is much smaller. It is found in Fig. 5(a), the open-loop Bode plot, that the magnitude with the PID controller is much larger. In this plot, the magnitude is defined as twenty times as many as denary logarithm of amplitude. This means the amplitude with the PID controller is larger. Larger amplitude makes it have a better capability to follow the input command in low frequency band while have a poorer suppression on noise in high frequency band. Fig. 5(b) is the close-loop Bode plot and it contains two key points. Firstly, the magnitude in low frequency is closer to 0 with PID controller, which means the amplitude in low frequency is closer to 1 and the steady-state error is smaller. Then, the cut-off frequency is higher under the effect of the controller, which results in a wider bandwidth and a faster response. However, wider bandwidth leads to worse robustness. Calculated phase margin demonstrates that the system with the PID controller is stable as shown in Fig. 6.

$$A_0 = \begin{bmatrix} -205.8824 & -2.1902e4 \\ 1.7495e4 & -1.2568e7 \end{bmatrix}, B_0 = \begin{bmatrix} 588.2353 \\ 0 \end{bmatrix},$$
$$C_0 = \begin{bmatrix} 0 & 1 \end{bmatrix}, D_0 = 0$$

In the following part, verification will be carried out to prove that the designed controller can guarantee the stability and robustness of the linearized systems at other operating points.

Fig. 1 and Fig. 2 demonstrate that the maximum gap metric appears between the lowest operating point and full working condition. This can also be deduced by looking at the matrices A, B, C, and D of the linearized systems. All of them have the same matrices B, C, and D. The only difference appears in matrix A. The expression of A_{22} in matrix A is $A_{22} = -\frac{f_m}{J_m} - \frac{60kn_r}{\pi \dot{m}_r J_m} x_2|_{x_2=x_{2,0}}$. As x_2 actually denotes $\dot{m}$, A_{22} is a monotonic function of the mass flow rate. The greater the difference is in the mass flow rate, the bigger the gap metric is. Therefore, four operating points are chosen and the amplitude- and phase-frequency characteristics are analyzed in the following. At each operating point, the state-space matrices of the linearized system are listed below, and the step response as well as Bode plot are shown in Fig. 7-10. Subscription 1, 2, 3, and 4 denote the working conditions of $\dot{m} = 0.57$ kg/s, $\dot{m} = 0.12$ kg/s, $\dot{m} = 0.03$ kg/s, and $\dot{m} = 0$, respectively.

$$A_1 = \begin{bmatrix} -205.8824 & -2.1902e4 \\ 1.7495e4 & -5.3070e6 \end{bmatrix}, B_1 = \begin{bmatrix} 588.2353 \\ 0 \end{bmatrix},$$
$$C_1 = \begin{bmatrix} 0 & 1 \end{bmatrix}, D_1 = 0$$
$$A_2 = \begin{bmatrix} -205.8824 & -2.1902e4 \\ 1.7495e4 & -1.1181e6 \end{bmatrix}, B_2 = \begin{bmatrix} 588.2353 \\ 0 \end{bmatrix},$$
$$C_2 = \begin{bmatrix} 0 & 1 \end{bmatrix}, D_2 = 0$$
$$A_3 = \begin{bmatrix} -205.8824 & -2.1902e4 \\ 1.7495e4 & -2.8026e5 \end{bmatrix}, B_3 = \begin{bmatrix} 588.2353 \\ 0 \end{bmatrix},$$
$$C_3 = \begin{bmatrix} 0 & 1 \end{bmatrix}, D_4 = 0$$
$$A_4 = \begin{bmatrix} -205.8824 & -2.1902e4 \\ 1.7495e4 & -1000 \end{bmatrix}, B_4 = \begin{bmatrix} 588.2353 \\ 0 \end{bmatrix},$$
$$C_4 = \begin{bmatrix} 0 & 1 \end{bmatrix}, D_4 = 0$$

From the data listed in Table 1, we can find that the PID controller designed according to full working condition can stabilize the linearized systems at other operating points as the phase margins are greater than 0, though the step responses began to oscillate with the decrease of the mass flow rate as the gap metrics between two linearized systems are getting bigger and the differences are more obvious as plotted in Fig. 7-10. It has mentioned that when $\dot{m}$ changes from 0 kg/s to 0.03 kg/s, the gap metrics have a substantial increase. Therefore, the step response of the linearized system at $\dot{m} = 0$ has significant oscillation. The oscillation occurred can also be explained by close loop Bode plots presented in Fig. 11-14, especially when the mass flow rate is relatively small. As shown in Fig. 13(b), there is a resonance peak appearing in the

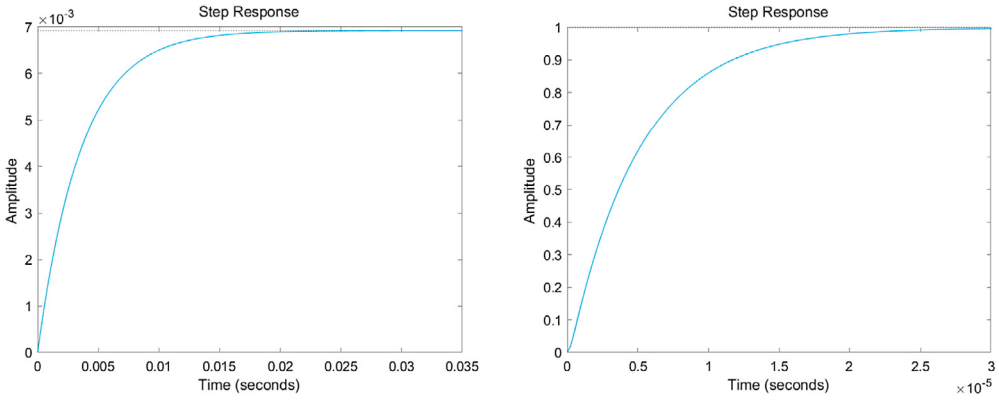

(a) Without the PID controller (b) With the PID controller

Fig. 7. Step responses of the linearized system at the working condition of $\dot{m} = 0.57$ kg/s.

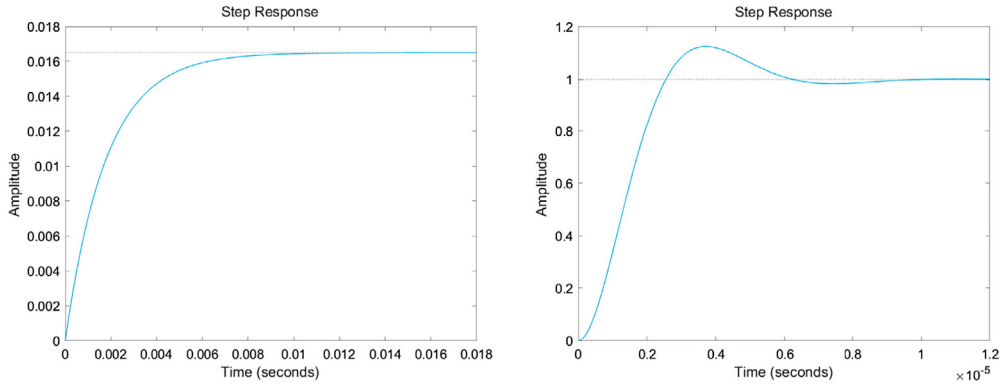

(a) Without the PID controller (b) With the PID controller

Fig. 8. Step responses of the linearized system at the working condition of $\dot{m} = 0.12$ kg/s.

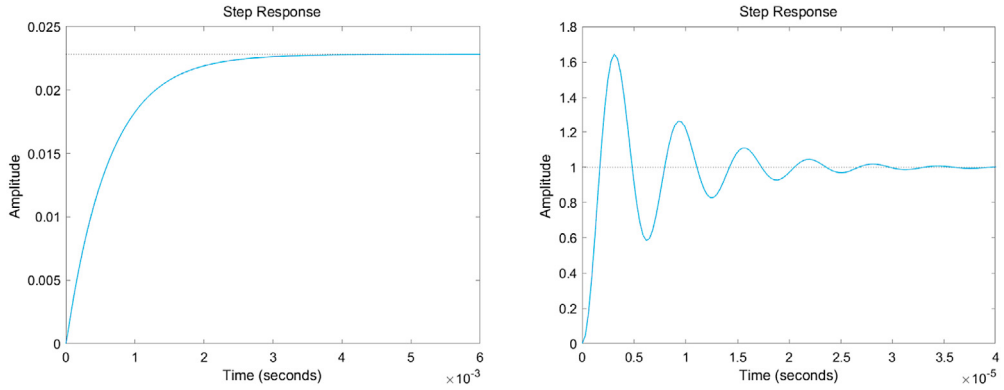

(a) Without the PID controller (b) With the PID controller

Fig. 9. Step responses of the linearized system at the working condition of $\dot{m} = 0.03$ kg/s.

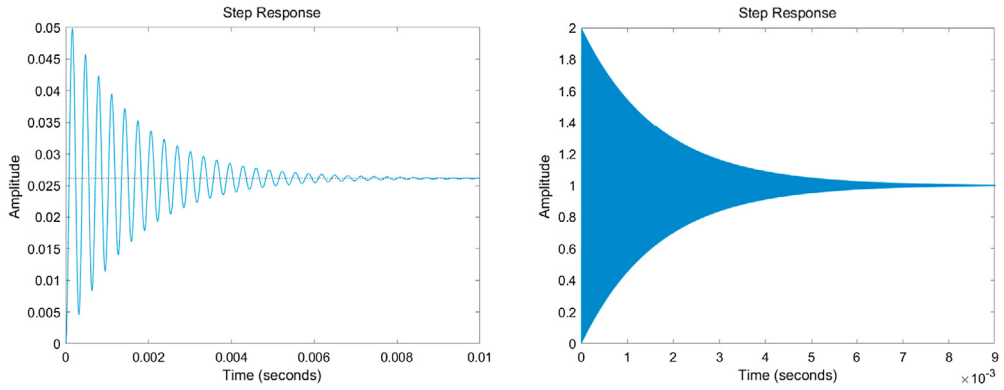

(a) Without the PID controller (b) With the PID controller

Fig. 10. Step responses of the linearized system at the working condition of $\dot{m} = 0$.

curve in red dash line which represents the system with the PID controller while the curve plotted in blue solid line has no peak. In spite of reducing settling time by increasing bandwidth, the system tends to be unstable with designed PID controller at the condition of low mass flow rate. In Fig. 14(b), both two curves have resonance peaks while the peak in the curve plotted in red dash line is more obvious than that in blue solid line, which results in a more severe oscillation in the step response as plotted in Fig. 10.

The poles and zeros of the systems can be obtained, which are listed in Table 2. Except for the linearized system at $\dot{m} = 0$, systems without the PID controller have a dominant pole on the order of 1e2 or 1e3. When the PID controller is applied, two more poles are

Table 1
Magnitude and phase margins at different operating points.

$\dot{m}$, kg·s^{-1}	Magnitude margin, dB	Phase margin, deg
0.57	Inf	88
0.12	Inf	55.8
0.03	Inf	15.7
0	Inf	0.0681

added as well as two zeros. Pole-zero cancellation happens in such a situation and the amount of the poles in fact is two. The PID controller makes the poles to be assigned. As the dominant pole of the system with the PID controller is farther from the imaginary axis, which is on the order of 1e4 or 1e5, than that of the system without the PID controller, the system with the PID controller has a faster response. As the poles of the linearized systems with the PID controller at $\dot{m} = 0.03$ kg/s and $\dot{m} = 0.12$ kg/s are conjugate complex roots, the step responses have oscillation to varying degrees.

4.2. Gain-scheduling linear quadratic regulation controller

The gain-scheduling linear quadratic regulation (LQR) controller is considered as a good controller because of its great performance and robustness against plant uncertainties [22]. Therefore, many researches focus on LQR control. Gain-scheduling LQR controllers were designed aiming at reducing the possibility of the occurrence of a type of accident [23]. This type of accident is known as rollover which is possibly due to the large lateral acceleration by excessive steering at high speed. As the vehicle speed varies, the controller gains changed with the speed of the vehicle. Similar to this situation, the mass flow rate during throttling process is changing thus it is possible to apply an gain-scheduling LQR controller to our study. The polynomial regression model-based gain-scheduling approach was proposed [24]. This approach improved performance and addressed computational drawbacks of conventional gain-scheduling methods. Meanwhile, the LQR controller provided good performance guarantees under slow and fast varying loads in cloud computing systems [25] and control of a floating offshore wind turbine above rated wind speed [26]. In reference [27], the LQR controller was designed for a novel concept of a co-axial bi-rotor UAV for planar motion control. Besides, LQR controllers were adopted to achieve simultaneous control of the quadcopter as well as its manipulator [28] and overcome challenges in controlling a Aerial Manipulation Systems (AMS) [29].

Eq. (20) can be written as follows,

$$\Delta\dot{x}_1 = A_{11}\Delta x_1 + A_{12}\Delta x_2 + B_{11}\Delta u \tag{23}$$

$$\Delta\dot{x}_2 = A_{21}\Delta x_1 + A_{22}\Delta x_2 \tag{24}$$

where $A_{11} = -\frac{R_m}{L_m}$, $A_{12} = -\frac{\pi n_r C_e}{30\dot{m}_r L_m}$, $A_{21} = \frac{30\dot{m}_r C_m}{\pi n_r J_m}$, $A_{22} = -\frac{f_m}{J_m} - \frac{60kn_r}{\pi\dot{m}_r J_m}x_2$, and $B_{11} = \frac{1}{L_m}$. Define

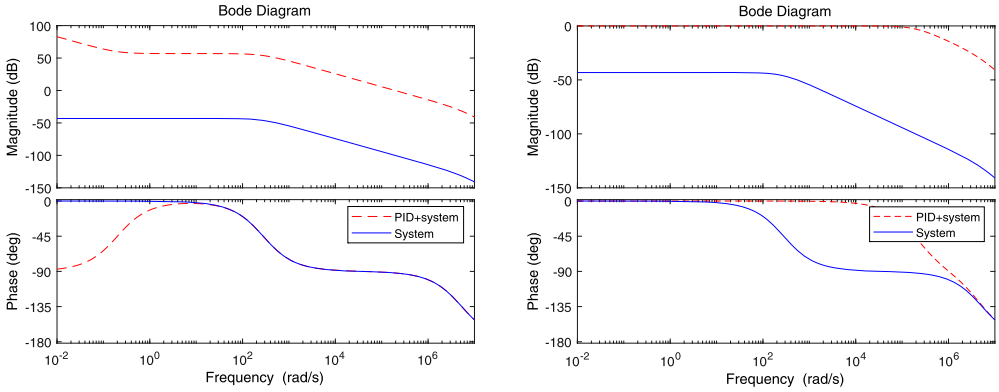

(a) Open loop Bode plot (b) Close loop Bode plot

Fig. 11. Bode plots of the linearized system at the working condition of $\dot{m} = 0.57$ kg/s.

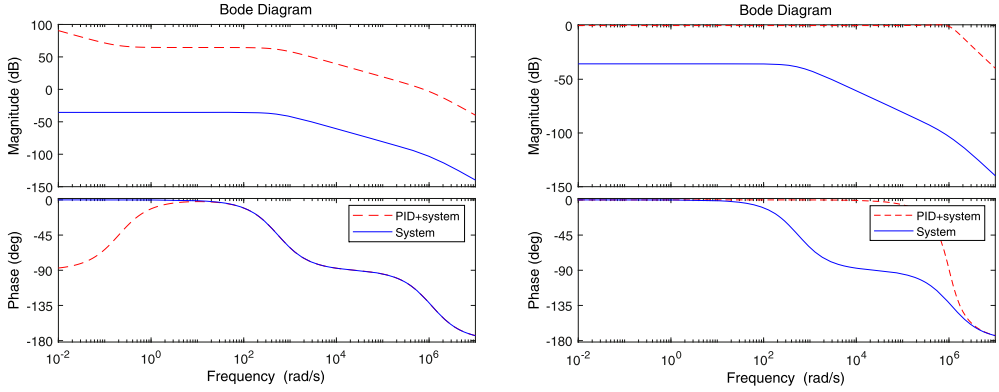

(a) Open loop Bode plot (b) Close loop Bode plot

Fig. 12. Bode plots of the linearized system at the working condition of $\dot{m} = 0.12$ kg/s.

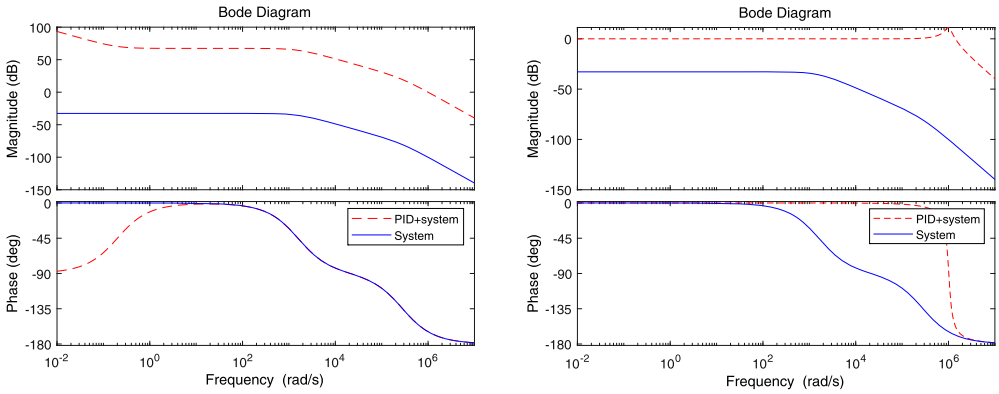

(a) Open loop Bode plot (b) Close loop Bode plot

Fig. 13. Bode plots of the linearized system at the working condition of $\dot{m} = 0.03$ kg/s.

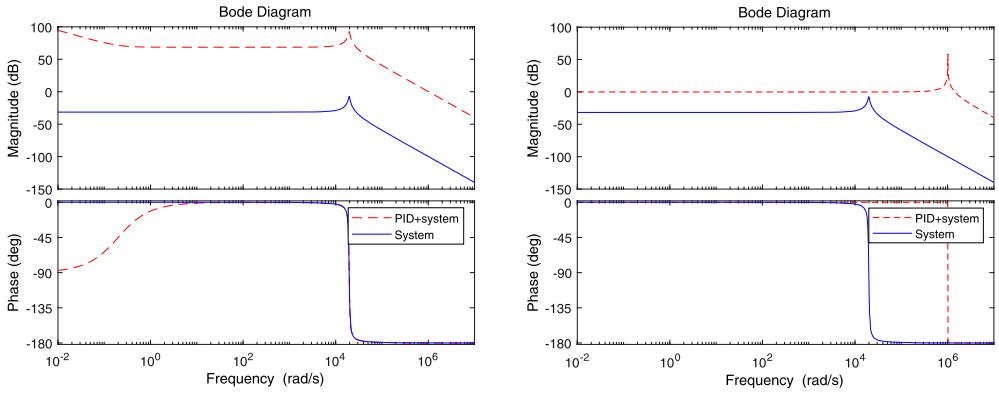

(a) Open loop Bode plot (b) Close loop Bode plot

Fig. 14. Bode plots of the linearized system at the working condition of $\dot{m} = 0$.

Table 2
Zeros and poles of systems.

Linearized system at	Without PID controller		With PID controller	
	Zeros	Poles	Zeros	Poles
$\dot{m} = 1.35$ kg·s^{-1}	None	-1.2568e7; -236.3712	-99.9499; -0.2	-1.2486e7; -8.2704e4; -99.95; -0.1994
$\dot{m} = .057$ kg·s^{-1}	None	-5.3069e6; -278.0881	-99.9499; -0.2	-5.1052e6; -2.0197e5; -99.95; -0.1997
$\dot{m} = 0.12$ kg·s^{-1}	None	-1.1178e6; -548.7530	-99.9499; -0.2	-5.5915e5+8.4711e5i; -5.5915e5-8.4711e5i; -99.9499; -0.1999
$\dot{m} = 0.03$ kg·s^{-1}	None	-2.7889e5; -1.5809e3	-99.9499; -0.2	-1.4023e5+1.0052e6i; -1.4023e5-1.0052e6i; -99.9499; -0.1999
$\dot{m} = 0$	None	-6.0294e2+1.9571e4i; -6.0294e2-1.9571e4i	-99.9499; -0.2	-6.0287e2+1.0149e6; -6.0287e2-1.0149e6i; -99.9499; -0.1999

$$e = x_{2d} - x_2 \tag{25}$$

where x_{2d} is the desired output, i.e., the mass flow rate reference, and e is the error between the real output and desired one. The increment of the error and its derivation can be expressed as follows,

$$\Delta e = -\Delta x_2 \tag{26}$$

$$\Delta \dot{e} = -\Delta \dot{x}_2 \tag{27}$$

Substitute with Eq. (26) and (27), Eq. (23) and (24) can be written as

$$\Delta \dot{x}_1 = A_{11}\Delta x_1 - A_{12}\Delta e + B_{11}\Delta u \tag{28}$$

$$\Delta \dot{e} = -A_{21}\Delta x_1 + A_{22}\Delta e \tag{29}$$

LQR controllers take the form,

$$\Delta u = -\mathbf{K}\Delta x = -\begin{bmatrix} k_1 & k_2 \end{bmatrix}\begin{bmatrix} \Delta x_1 \\ \Delta e \end{bmatrix} = -k_1\Delta x_1 - k_2\Delta e$$
$$= -k_1\Delta x_1 + k_2\Delta x_2 \tag{30}$$

The gain matrix $\mathbf{K}$ needs to be found that minimizes the value of the quadratic cost function [30]

$$J = \int_0^\infty \left(\Delta \mathbf{x}^T \mathbf{Q}\Delta \mathbf{x} + \Delta u^T \mathbf{R}\Delta u\right) dt \tag{31}$$

where matrices $\mathbf{Q}$ and $\mathbf{R}$ are weighting matrices for state increment ($\Delta \mathbf{x}$) and control signal increment (Δu), respectively. In order to determine $\mathbf{K}$, the following Riccati equation should be solved

$$\mathbf{PA} + \mathbf{A}^T\mathbf{P} - \mathbf{PBR}^{-1}\mathbf{B}^T\mathbf{P} + \mathbf{Q} = 0 \tag{32}$$

Finally, the controller gain matrix $\mathbf{K}$ is computed by

$$\mathbf{K} = \mathbf{R}^{-1}\mathbf{B}^T\mathbf{P} \tag{33}$$

By solving Riccati equation, the gain matrix obtained to minimize the linear quadratic cost function, i.e., lowest cumulative error and input energy, makes the LQR controller to be optimal. In this paper, matrices $\mathbf{Q}$ and $\mathbf{R}$ are given as follows,

$$\mathbf{Q} = \begin{bmatrix} 100 & 0 \\ 0 & 1000 \end{bmatrix}$$
$$\mathbf{R} = 0.01$$

As the mass flow rate is changing during throttling process, the controller gains should be determined by considering the mass flow rate provided by the pump. Gain-scheduling adaptive system is adopted here. In this way, $\mathbf{K}$ in Eq. (30) could actually be described by $\mathbf{K} = \mathbf{K}(\dot{m})$. For every desired mass flow rate, the LQR equation should be applied to determine all controller gains. For each input voltage, there is a corresponding mass flow rate which contributes to a $\mathbf{K}$ accordingly. Several working conditions are selected and the $\mathbf{K}$ matrices are listed in Table 3. Other $\mathbf{K}$ matrices can be obtained by means of a looking up table and interpolation.

With a LQR controller, the eigenvalues, i.e., pole locations, change significantly. In the following, the conditions listed in Table 4 are divided into two regimes. One is overdamped and the eigenvalues distribute on the negative real axis. The other is underdamped, in which the eigenvalues are conjugate roots in left-half complex plane.

When the system is overdamped, there are two negative real roots. The root closer to imaginary axis is the dominant pole and determines the response of the system. Under the effect of the LQR controller, the dominant pole moves away from the imaginary axis, which is illustrated in Fig. 15. It makes the system respond more quickly and maintain robustness against the disturbance. Instead, the controller has little influence on the other pole.

As shown in Fig. 16, when the LQR controller is applied, the damping ratio increases from 0.03 to 0.752 in the underdamped condition, which increases the ability to suppress the disturbance. Meanwhile, the conjugate poles moving away from the imaginary axis in left-half complex plane improve the dynamic response of the system.

Table 3
K matrices at typical working conditions.

U,V	$\dot{m}$, kg·s^{-1}	**K**
0	0	[257.3978, -948.7436]
1	0.0252	[116.8259, -62.7086]
10	0.1839	[99.7879, -0.4619]
50	0.5595	[99.5832, 0.2265]
100	0.8553	[99.5937, 0.1914]
150	1.0848	[99.6016, 0.1646]
220	1.35	[99.6089, 0.1404]

Table 4
Eigenvalues at typical working conditions.

$\dot{m}$, kg·s^{-1}	Without LQR controller	With LQR controller
	Eigenvalues	Eigenvalues
0	-6.0294e2±1.9571e4i	-7.6308e4±6.6899e4i
0.0252	-1.8452e3; -2.3394e5	-7.5346e4; -2.2916e5
0.1839	-429.6405; -1.7127e6	-5.9139e4; -1.7217e6
0.5595	-279.4429; -5.2092e6	-5.8858e4; -5.2092e6
0.8553	-254.0046; -7.9628e6	-5.8839e4; -7.9628e6
1.0848	-243.8246; -1.0099e7	-5.8833e4; -1.0099e7
1.35	-236.3715; -1.2568e7	-5.8830e4; -1.2568e7

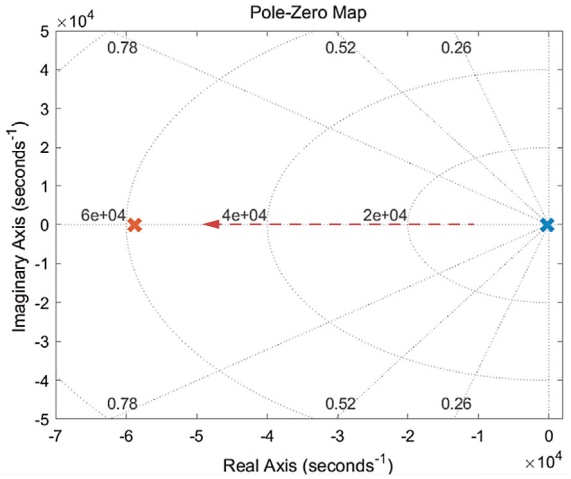

Fig. 15. Root locus for an overdamped system.

5. Results and discussions

The electric pump model is implemented in Matlab/Simulink. The simulation results are presented in the following sections including validation of the controllers and simulation on throttling process. It is worth mentioning that during the throttling period, the change process can be done instantly while the different operating conditions are required to be maintained for a long time. In order to save computing resources and time, the duration on steady state of throttling process for simulation is shortened, which simply intends to show the control effect on the dynamic process.

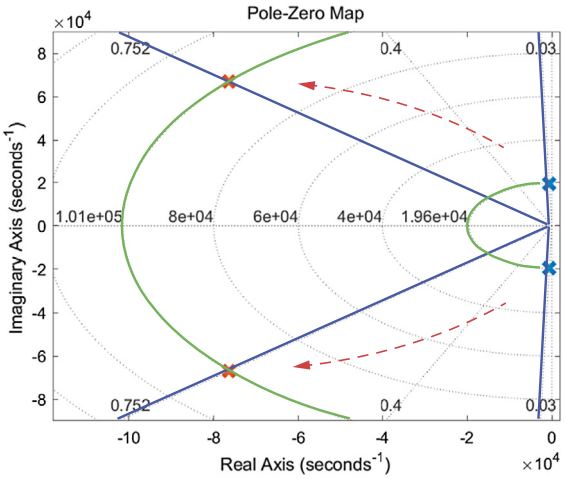

Fig. 16. Root locus for an underdamped system.

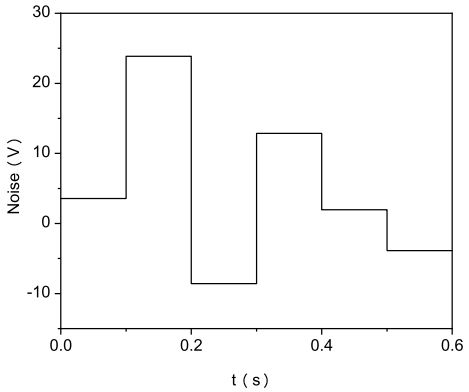

Fig. 17. Disturbance in validation.

5.1. Controller validation

A sequence of step signals is used as the validation input. In validation, two group simulations are conducted. One is the step signal set, the other is step signal set with disturbance. The disturbance sequence is shown in Fig. 17. In each simulation group, the PID controller and LQR gain-scheduling controllers are tested on the original nonlinear system. Comparison between simulation results and the desired value are presented in Fig. 18.

Fig. 18(a) shows that both the PID and LQR gain-scheduling controllers improve the dynamic response and reduce the rise time. Meanwhile the controllers guarantee the steady state value. When the disturbance in Fig. 17, which the variance is 100 V^2, is injected, as illustrated in Fig. 18(b), it is obvious that the electric pump system without a controller behaves abnormally and suffers a deviation from the designed value. While the systems with controllers still have good performance on both the dynamic response and steady state value. The changes of the system response under the effect of controllers are relatively small, which can be seen in Fig. 19. Except for the sudden change of the signal, the errors between the system with and without disturbance are limited in 2%. The root mean square errors (RMSEs) of the two controllers are calculated and the results are listed in Table 5. The RMSEs show that the PID and LQR gain-scheduling controllers have the same control effect in total.

In practical applications, a controller not only needs to stabilize the system, the control signal may also need to satisfy the operating requirements of the controlled objects. The control signals exerted to obtain the results shown in Fig. 18 are presented in

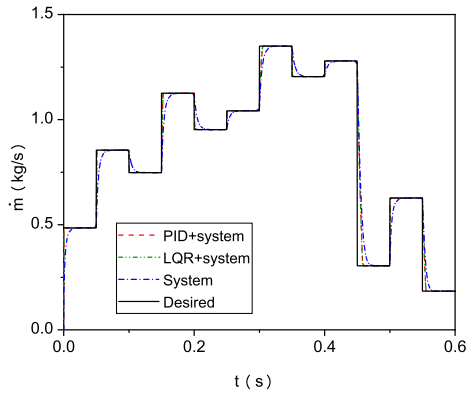

(a) No disturbance

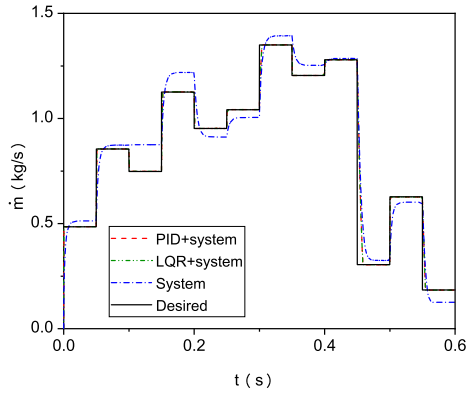

(b) With disturbance

Fig. 18. Influence of controllers on fuel mass flow rate in validation.

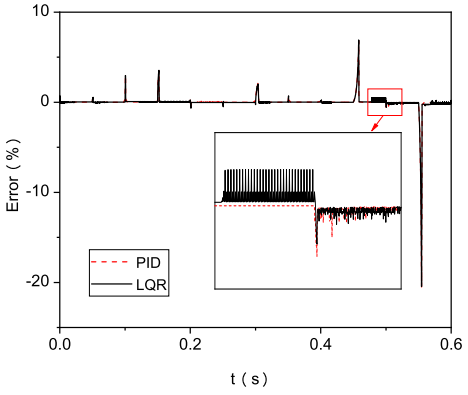

Fig. 19. Errors between the system with and without disturbance under the effect of controllers in validation.

Table 5
RMSEs of controllers in validation ($kg \cdot s^{-1}$).

	Without disturbance	With disturbance
No controller	8.34e-2	9.77e-2
PID	6.68e-2	6.66e-2
LQR	6.68e-2	6.66e-2

Fig. 20. Oscillations can be found in the figure which illustrate in red dash dot line, especially when there is disturbance during the operation. It means that although the PID controller has the same control effect as the LQR gain-scheduling controller, it needs vio-

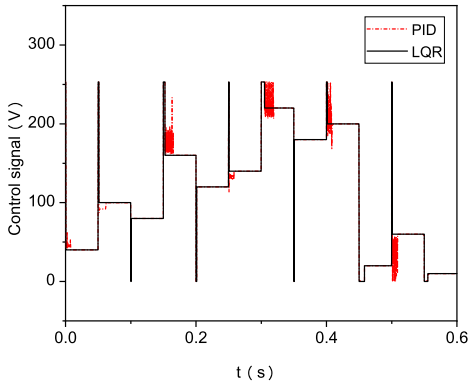

(a) No disturbance

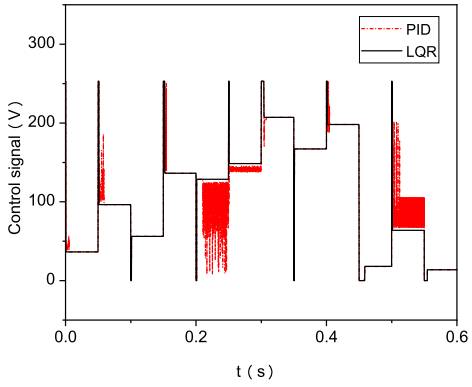

(b) With disturbance

Fig. 20. Control signal behavior in validation.

lent oscillations in the input signal to compensate the error with respect to the reference value. However, this kind of oscillations is detrimental to the lifespan of the electric pump. On the contrary, the signal produced by the LQR gain-scheduling controller seems much smoother and it is better for mitigation and life extension of the electric pump.

5.2. Simulation considering throttling process

Last section proves that the controllers can track the target curve, which only has step signals, even if there is disturbance. However, there are periods that the mass flow rate needs to change continuously and gradually in throttling process, which means the controllers need be able to track ramp signals. In the following, a mixed signal set considering the throttling process is applied in the simulation. The signal sequence lasts 0.3 second, which includes full working condition, other working conditions, and the continuous regulating process.

Same as the validation, two group simulations are conducted. One is the mixed signal set, the other is the mixed signal set with disturbance. The disturbance sequence is shown in Fig. 21.

Similar to simulation results shown in validation section, no matter whether there is disturbance or not, controllers improve the dynamic response and reduce the rise time in throttling process as shown in Fig. 22. Meanwhile the controllers make the system work at desired steady state. The notable deficiency is that during the ramp signal process, i.e., the mass flow rate continuous reducing period, the controllers have errors when tracking the target curve. In contrast, the PID controller has a better performance on tracking ramp signal. This can be explained from Fig. 22(b). The PID

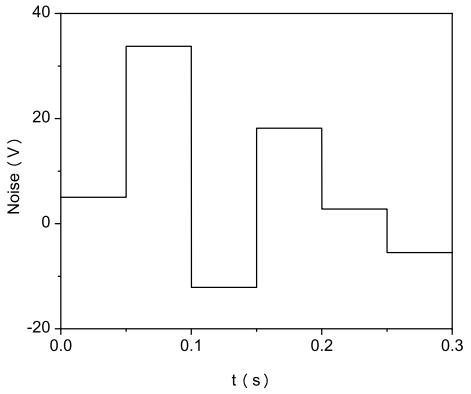

Fig. 21. Disturbance in throttling process.

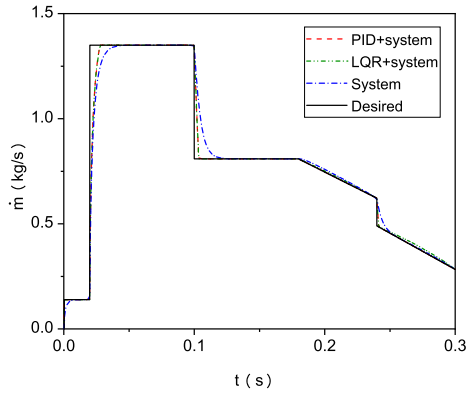

(a) No disturbance

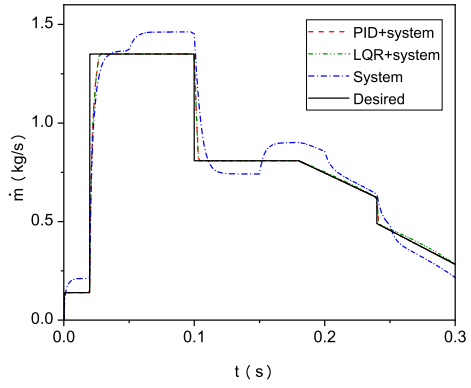

(b) With disturbance

Fig. 22. Influence of controllers on fuel mass flow rate in throttling process.

controller changed the control signal frequently to try to compensate the discrepancy with the desired value. On the other hand, the PID controller has less errors during the whole throttling process, which is more obvious than that in validation section, especially at the beginning of the simulation as shown in Fig. 23. The RMSEs (Root Mean Square Errors) of the two controllers are calculated and the results are listed in Table 6. The RMSEs show that the PID controller has better control effect in total on throttling process.

However, Fig. 24(b) demonstrated the control signal generated by the PID controller on throttling process has severer oscillation compared with signals generated by the LQR controller as well as signals produced by the PID controller in validation section.

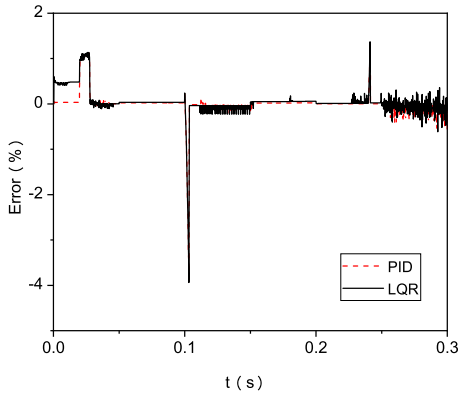

Fig. 23. Errors between the system with and without disturbance under the effect of controllers in throttling process.

Table 6
RMSEs of controllers in simulation on throttling process ($kg{\cdot}s^{-1}$).

	Without disturbance	With disturbance
No controller	8.84e-2	1.13e-1
PID	7.12e-2	7.00e-2
LQR	7.14e-2	7.02e-2

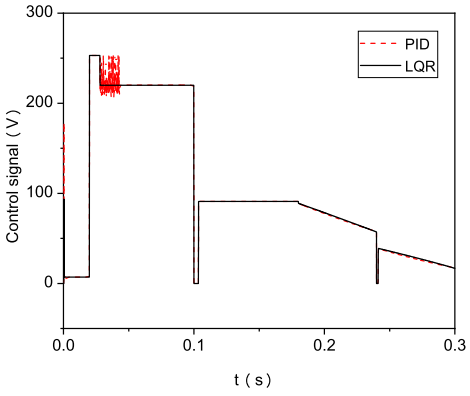

(a) No disturbance

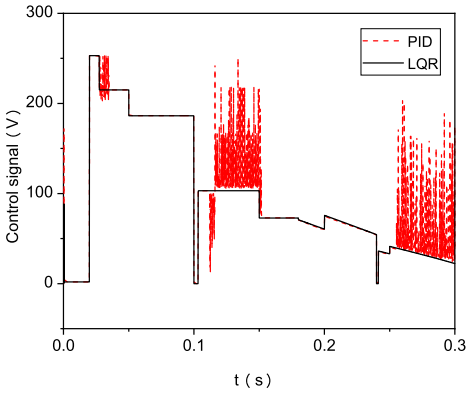

(b) With disturbance

Fig. 24. Control signal behavior in throttling process.

6. Conclusions

System analysis and controller design of the electric pump considering the application on deep throttling rocket engine is described in this paper. The proportional-integral-derivative controller and gain-scheduling linear quadratic regulator are adopted to stabilize the system and track the target curves. The main conclusions are drawn as follows:

(1) Though it demonstrates that the electric pump system behaves nonlinearly due to a quadratic term in the dynamics equation, the analysis of the gap metric shows that the system control problem can be solved by a linear controller.
(2) By analyzing the amplitude- and phase-frequency characteristics as well as the pole-zero distribution of the system with and without controllers, it theoretically proves the designed proportional-integral-derivative controller and gain-scheduling linear quadratic regulator can stabilize the linearized equations in incremental form at different operating points. This indicates that these two controllers are available for the original system in the whole range of working conditions.
(3) Simulations conducted to test the effect of the controllers show that designed proportional-integral-derivative controller has a better control effect on the system especially when to track ramp signals. However, the control signal produced by the proportional-integral-derivative controller seems hard to be implemented as there are severe oscillations during the tracking process. Meanwhile, the parameter tuning of the proportional-integral-derivative controller depends on quite rich engineering experience. Considering the above two reasons, the gain-scheduling linear quadratic regulator seems better.

Further investigation may consider the linear or nonlinear model predictive control method, as when tracking the ramp signal, there are relative errors with a gain-scheduling linear quadratic regulator and severe oscillations with a proportional-integral-derivative controller which may be due to the nonlinearity of the system.

Declaration of competing interest

The authors declare that they have no known competing financial interests or personal relationships that could have appeared to influence the work reported in this paper.

Acknowledgements

This research was sponsored by the National University of Defense Technology. The support provided by China Scholarship Council (grant number 201903170197) during a visit of Runsheng Hu to Delft University of Technology is acknowledged. Meanwhile, all the staff and fellow researchers providing technical and academic support are also greatly appreciated.

References

[1] G.P. Sutton, History of liquid propellant rocket engines in the United States, J. Propuls. Power 19 (6) (2003) 978–1007.
[2] B. Zhao, N. Yu, Y. Liu, P. Zeng, J. Wang, Unsteady simulation and experimental study of hydrogen peroxide throttleable catalyst hybrid rocket motor, Aerosp. Sci. Technol. 76 (2018) 27–36.
[3] Y. Jin, X. Xu, Q. Yang, S. Zhu, Numerical investigation of flame appearance and heat flux and in a deep-throttling variable thrust rocket engine, Aerosp. Sci. Technol. 88 (2019) 457–467.
[4] Z. Zhang, S. Gong, J. Li, The fuel-optimal trajectory for finite-thrust lunar ascent, Aerosp. Sci. Technol. 39 (2014) 675–684.
[5] M.J. Casiano, J.R. Hulka, V. Yang, Liquid-propellant rocket engine throttling: a comprehensive review, J. Propuls. Power 26 (5) (2010) 897–923.
[6] K. Radhakrishnan, M. Son, K. Lee, J. Koo, Effect of injection conditions on mixing performance of pintle injector for liquid rocket engines, Acta Astronaut. 150 (2018) 105–116.

[7] X.-x. Fang, C.-b. Shen, Study on atomization and combustion characteristics of LOX/methane pintle injectors, Acta Astronaut. 136 (2017) 369–379.
[8] M. Son, K. Radhakrishnan, J. Koo, O.C. Kwon, H.D. Kim, Design procedure of a movable pintle injector for liquid rocket engines, J. Propuls. Power 33 (4) (2017) 858–869.
[9] N. Soldà, D. Lentini, Opportunities for a liquid rocket feed system based on electric pumps, J. Propuls. Power 24 (6) (2008) 1340–1346.
[10] G. Johnsson, M. Bigert, Development of small centrifugal pumps for an electric propellant pump system, Acta Astronaut. 21 (6–7) (1990) 429–438.
[11] H.-D. Kwak, S. Kwon, C.-H. Choi, Performance assessment of electrically driven pump-fed LOX/kerosene cycle rocket engine: comparison with gas generator cycle, Aerosp. Sci. Technol. 77 (2018) 67–82.
[12] V. Petrucha, P. Ripka, V. Grim, V. Petrucha, P. Ripka, M. Havlena, A. Torii, T. Pajdla, Rotational speed measurement and angular position reference for a cryogenic propellant electric pump, J. Electr. Eng. (Elektrotechnicky Casopis) 66 (7) (2015) 199–202.
[13] P.P. Rachov, H. Tacca, D. Lentini, Electric feed systems for liquid-propellant rockets, J. Propuls. Power 29 (5) (2013) 1171–1180.
[14] T.T. Georgiou, M.C. Smith, Optimal robustness in the gap metric, in: Proceedings of the 28th IEEE Conference on Decision and Control, IEEE, 1989, pp. 2331–2336.
[15] S. Saki, H. Bolandi, et al., Optimal direct adaptive soft switching multi-model predictive control using the gap metric for spacecraft attitude control in a wide range of operating points, Aerosp. Sci. Technol. 77 (2018) 235–243.
[16] K.H. Ang, G. Chong, Y. Li, PID control system analysis, design, and technology, IEEE Trans. Control Syst. Technol. 13 (4) (2005) 559–576.
[17] S. Razvarz, C. Vargas-Jarillo, R. Jafari, A. Gegov, Flow control of fluid in pipelines using PID controller, IEEE Access 7 (2019) 25673–25680.
[18] Y. Govdeli, S. Moheed Bin Muzaffar, R. Raj, B. Elhadidi, E. Kayacan, Unsteady aerodynamic modeling and control of pusher and tilt-rotor quadplane configurations, Aerosp. Sci. Technol. 94 (2019) 105421.
[19] Q. Yin, J.Z. Jiang, S.A. Neild, H. Nie, Investigation of gear walk suppression while maintaining braking performance in a main landing gear, Aerosp. Sci. Technol. 91 (2019) 122–135.
[20] H. Habibi, H.R. Nohooji, I. Howard, Adaptive PID control of wind turbines for power regulation with unknown control direction and actuator faults, IEEE Access 6 (2018) 37464–37479.
[21] Y. Song, X. Huang, C. Wen, Robust adaptive fault-tolerant PID control of mimo nonlinear systems with unknown control direction, IEEE Trans. Ind. Electron. 64 (6) (2017) 4876–4884.
[22] L.M. Argentim, W.C. Rezende, P.E. Santos, R.A. Aguiar PID, LQR and LQR-PID on a quadcopter platform, in: 2013 International Conference on Informatics, Electronics and Vision (ICIEV), IEEE, 2013, pp. 1–6.
[23] V.F. Dal Poggetto, A.L. Serpa, Vehicle rollover avoidance by application of gain-scheduled LQR controllers using state observers, Veh. Syst. Dyn. 54 (2) (2016) 191–209.
[24] Y. Choi, H. Jimenez, D.N. Mavris, Statistical gain-scheduling method for aircraft flight simulation, Aerosp. Sci. Technol. 46 (2015) 493–505.
[25] P.S. Saikrishna, R. Pasumarthy, N.P. Bhatt, Identification and multivariable gain-scheduling control for cloud computing systems, IEEE Trans. Control Syst. Technol. 25 (3) (2016) 792–807.
[26] O. Bagherieh, R. Nagamune, Gain-scheduling control of a floating offshore wind turbine above rated wind speed, Control Theory Technol. 13 (2) (2015) 160–172.
[27] S. Darvishpoor, J. Roshanian, M. Tayefi, A novel concept of vtol bi-rotor uav based on moving mass control, Aerosp. Sci. Technol. 107 (2020) 106238.
[28] H. Bonyan Khamseh, S. Ghorbani, F. Janabi-Sharifi, Unscented Kalman filter state estimation for manipulating unmanned aerial vehicles, Aerosp. Sci. Technol. 92 (2019) 446–463.
[29] Z. Samadikhoshkho, S. Ghorbani, F. Janabi-Sharifi, K. Zareinia, Nonlinear control of aerial manipulation systems, Aerosp. Sci. Technol. 104 (2020) 105945.
[30] A. Moutinho, J.R. Azinheira, E.C. de Paiva, S.S. Bueno, Airship robust path-tracking: a tutorial on airship modelling and gain-scheduling control design, Control Eng. Pract. 50 (2016) 22–36.